Formation of deeply bound kaonic atoms in (K^-, N) reactions

J. Yamagata,[1] H. Nagahiro,[2] R. Kimura,[1] and S. Hirenzaki[1]

[1]*Department of Physics, Nara Women's University, Nara 630-8506, Japan*
[2]*Research Center for Nuclear Physics (RCNP), Osaka University, Ibaraki, Osaka 567-0047, Japan*
(Received 3 July 2007; published 31 October 2007)

We study theoretically the (K^-, N) reactions for the formation of the deeply bound kaonic atoms, which were predicted to be quasistable with narrow widths, using the Green's function method. We systematically consider various cases with different target nuclei and energies and find clear signals in the theoretical spectra for all cases considered in this article. The signals show very interesting structures, such as a *RESONANCE DIP* instead of a resonance peak. We discuss the origins of the interesting structures and the possibilities of obtaining new information on the existence of kaonic nuclei from the spectra of atomic state formations.

I. INTRODUCTION

Kaonic atoms and kaonic nuclei carry important information concerning the K^--nucleon interaction in the nuclear medium. This information is very important in understanding kaon properties at finite density and, for example, to determine the constraints on kaon condensation in high-density matter.

First, we need to clarify the differences between kaonic atoms and kaonic nuclei. The kaonic nuclei are kaon-nucleus bound systems by way of the strong interactions inside the nucleus and are controversial objects, as described in Refs. [1–3]. We simply mention here that some indications of the existence of the *NARROW* kaonic nuclear states reported in Ref. [4] were withdrawn by the authors in recent conference talks [5]. On the other hand, the kaonic atoms are the Coulomb-assisted kaon-nucleus bound systems which were theoretically predicted to be quasistable by the realistic kaon-nucleus optical potentials. Thus, the kaonic atoms are expected to be observed by proper reactions. Actually, shallow atomic states have been observed experimentally by kaonic x-ray spectroscopy for a long time. In the beginning of Sec. III, we show two figures to explain the quantitative differences between kaonic atoms and kaonic nuclei. In this article, we consider mainly the deeply bound kaonic atoms, which cannot be observed by the standard x-ray spectroscopy.

In this article, we study in-flight (K^-, N) reactions systematically using the Green's function method [6] for the formation of kaonic atoms. The Green's function method is known to be suited for evaluating the formation rates of both stable and unstable bound systems. The (K^-, N) reaction for the $\bar{K}$-nucleus system formation was proposed in Refs. [7,8], and theoretical results of the reaction energy spectra were obtained in Ref. [9] using the same theoretical approach of Ref. [10] for the deeply bound pionic atom formation reaction [11,12], where we used the effective number approach [9], which is best suited for studying the formation of discrete states. Theoretical spectra were later obtained using the Green's function method in Ref. [13], where we showed the difficulties in experimentally obtaining clear signals for kaonic nuclear states formation. Similar theoretical calculations were also performed in Ref. [14]. In our previous paper [13], we also found simultaneously that there existed clear signals

for kaonic atom formation in the theoretical spectra which showed interesting structures such as *RESONANCE DIP*. We think the evaluation made in Refs. [9,13] is very interesting and important to knowing the experimental feasibilities of the (K^-, N) reaction and to understanding the deeper meaning of the observed spectra for both kaonic atom and kaonic nuclei formation [7,15].

The purpose of this article is to study thoroughly the atomic state formation spectra by (K^-, N) reactions. We consider various cases with different target nuclei and incident energies and show the calculated spectra. We then study the origins of the interesting structures of the spectra reported in this article and in Ref. [13], and we study the experimental feasibility. We also discuss the possibilities of obtaining new information on the kaon-nucleus interaction and the existence of kaonic nuclei from the (K^-, N) spectra of the atomic state formation. We believe that realistic calculations of the formation spectra are necessary for all observed results in order to study kaon properties in the nuclear medium and to obtain decisive conclusions. So far, experimental studies of the in-flight (K^-, N) reactions were proposed to search for kaonic nuclei and performed by Kishimoto and his collaborators [7,15]. Our calculated results for kaonic nuclei formation [9,13] are in good agreement with the data in Ref. [16], which do not show any clear peaks and were reported after our predictions.

The K^--nucleus interaction has been studied for a long time based on the lightly bound kaonic atom data obtained by x-ray spectroscopy. Very interesting features of kaon-nucleus bound systems are tied to the properties of kaons in nuclei which are strongly influenced by the change undergone by the $\Lambda(1405)$ in the nuclear medium, because the $\Lambda(1405)$ is a resonance state just below the kaon-nucleon threshold. [We refer to the $\Lambda(1405)$ generically although chiral theories predict two $\Lambda(1405)$ states [17] for which experimental evidence is claimed [18].] In fact, studies of kaonic atoms have been carried out by modifying the properties of the $\Lambda(1405)$ in the nuclear medium [19–21]. These works reproduce the properties of specific kaonic atoms reasonably well. In Ref. [22], a phenomenological study of kaonic atoms is performed comprehensively, where different density-dependent

potentials are considered for χ^2 fits in order to take into account possible nonlinear effects caused by the $\Lambda(1405)$ resonance.

Recently, there have been significant developments in the description of hadron properties in terms of the SU(3) chiral Lagrangian. The interpretation of the $\Lambda(1405)$ resonance state as a baryon-meson coupled system proposed in Ref. [23] is also supported by studies with the chiral Lagrangian [24,25]. Subsequently, the properties of $\Lambda(1405)$ in nuclear medium using the SU(3) chiral unitary model were also investigated by Waas *et al.* [26], Lutz [27], Ramos and Oset [28], and Cieplý *et al.* [29]. All these works considered the Pauli effect on the intermediate nucleons. In addition, in Ref. [27], the self-energy of the kaon in the intermediate states is considered, and in Ref. [28], the self-energies of the pions and baryons are also taken into account. An update of Ref. [28] considers also the effect of the p-wave self-energy [30], which, however, has a negligible effect in atoms [31]. These approaches lead to a kaon self-energy in the nuclear medium that can be tested with kaonic atoms and kaonic nuclei. The in-medium $\bar{K}$ properties have been studied also in Refs. [32,33] based on the meson-exchange Jülich $\bar{K}N$ interaction and in Ref. [34] for the environment in heavy ion collisions. These theoretical potentials are shown to have the ability to reproduce the kaonic atom data reasonably well [35,36]. The kaonic nuclear states were also studied using these interactions and shown to have large decay widths of the order of several tens of MeV [8,9,13,35,37,38].

In this work, we mainly use the phenomenological optical potential obtained in Ref. [22] and the microscopic chiral unitary optical potential obtained in Ref. [28] to investigate the structure and formation of deeply bound kaonic atoms. We also consider another type of phenomenological optical potential developed to take into account the two-body kaon absorption effects explicitly according to Ref. [38].

In Sec. II, we describe the theoretical models used to study the structure and formation of kaonic atoms. Numerical results are presented and discussed in Sec. III. In Sec. IV, we discuss the effects of the existence of kaonic nuclei in the spectra in the energy region of the atomic states formation and also discuss the origin of the interesting spectra shape of the atomic states formation. We give conclusions of this study in Sec. V.

II. FORMALISM

To investigate the structure and formation of the kaonic atoms theoretically, we consider the Klein-Gordon equation

$$[-\nabla^2 + \mu^2 + 2\mu V_{\text{opt}}(r)]\phi(r) = [\omega - V_{\text{coul}}(r)]^2\phi(r). \quad (1)$$

Here, μ is the kaon-nucleus reduced mass and $V_{\text{coul}}(r)$ is the Coulomb potential with a finite nuclear size:

$$V_{\text{coul}}(r) = -e^2 \int \frac{\rho_{\text{ch}}(r')}{|r - r'|}d^3r', \quad (2)$$

where $\rho_{\text{ch}}(r)$ is the charge distribution of the nucleus. We employ the empirical Woods-Saxon form for the density as

$$\rho_{\text{ch}}(r) = \frac{\rho_0}{1 + \exp[(r - R)/a]}, \quad (3)$$

where we use $R = 1.18A^{1/3} - 0.48$ fm and $a = 0.5$ fm, with A the nuclear mass number. To evaluate the kaon-nucleus optical potential, we use the point nucleon density distributions deduced from ρ_{ch} in Eq. (3) by the same prescription described in Sec. 4 in Ref. [39]. The shapes of the density distributions of the proton and neutron are assumed to be the same in this article. For the studies of the structure of the kaonic atoms, we solve the Klein-Gordon equation numerically, following the method of Oset and Salcedo [40]. The application of this method to pionic atom studies is reported in detail in Ref. [39].

We use the Green's function method [6] to calculate the formation cross sections of the $\bar{K}$-nucleus system in the (K^-, p) reactions. The details of the application of the Green's function method are found in Refs. [41–44].

The present method starts with a separation of the reaction cross section into the nuclear response function $S(E)$ and the elementary cross section of the $p(\bar{K}, p)\bar{K}$ with the impulse approximation

$$\left(\frac{d^2\sigma}{d\Omega dE}\right)_{A(\bar{K},p)(A-1)\otimes\bar{K}} = \left(\frac{d\sigma}{d\Omega}\right)_{p(\bar{K},p)\bar{K}}^{\text{lab}} \times S(E). \quad (4)$$

The forward differential cross section of the elementary process $p(\bar{K}, p)\bar{K}$ in the laboratory frame $(d\sigma/d\Omega)_{p(\bar{K},p)\bar{K}}^{\text{Lab}}$ is evaluated to be 8.8 mb/sr at $T_{\bar{K}} = 600$ MeV using the K^-p elastic cross-section data in Ref. [45]. We should mention here that the corrections to this evaluation were reported in Ref. [29], which reduce the elementary cross section to be 3.6 mb/sr effectively. In this article, we show all the calculated results assuming the elementary cross section to be 8.8 mb/sr.

The calculation of the nuclear response function with the complex potential is formulated by Morimatsu and Yazaki [6] in a generic form as

$$S(E) = -\frac{1}{\pi}\text{Im}\sum_f \tau_f^\dagger G(E)\tau_f, \quad (5)$$

where the summation is taken over all possible final states. The amplitude τ_f denotes the transition of the incident particle ($\bar{K}$) to the proton-hole and the outgoing ejectile (p), involving the proton-hole wave function ψ_{j_p} and the distorted waves χ_i and χ_f, of the projectile and ejectile, taking the appropriate spin sum; that is,

$$\tau_f(r) = \chi_f^*(r)\xi_{1/2,m_s}^*[Y_{l_{\bar{K}}}^*(\hat{r}) \otimes \psi_{j_p}(r)]_{JM}\chi_i(r), \quad (6)$$

with the meson angular wave function $Y_{l_{\bar{K}}}(\hat{r})$ and the spin wave function $\xi_{1/2,m_s}$ of the ejectile. The distorted waves are written with the distortion factor $F(r)$ as

$$\chi_f^*(r)\chi_i(r) = \exp(iq \cdot r)F(r), \quad (7)$$

with the momentum transfer q. The distortion factor $F(r)$ is defined as

$$F(r) = \exp\left(-\frac{1}{2}\bar{\sigma}\int_{-\infty}^{\infty}dz'\bar{\rho}(z', b)\right), \quad (8)$$

where $\bar{\sigma}$ is the averaged distortion cross section defined as

$$\bar{\sigma} = \frac{\sigma_{\bar{K}N} + \sigma_{pN}}{2}, \quad (9)$$

with the total cross sections of the incident kaon and emitted proton with the nucleons in the nucleus. The averaged nuclear density $\bar{\rho}(z', \boldsymbol{b})$ in Eq. (8) is defined as

$$\bar{\rho}(r) = \frac{\rho_0}{1 + \exp[(r - \bar{R})/\bar{a}]} \tag{10}$$

in the polar coordinates with the averaged radial parameter $\bar{R}$ and diffuseness parameter $\bar{a}$ defined as

$$\bar{R} = \frac{R_i + R_f}{2} \tag{11}$$

and

$$\bar{a} = \frac{a_i + a_f}{2}, \tag{12}$$

with the density parameters of the nuclei in the initial and final states.

Green's function $G(E)$ contains the kaon-nucleus optical potential in the Hamiltonian $H_{\bar{K}}$ as

$$G(E, \boldsymbol{r}, \boldsymbol{r}') = \langle p^{-1}|\phi_{\bar{K}}(\boldsymbol{r}) \frac{1}{E - H_{\bar{K}} + i\epsilon} \phi_{\bar{K}}^{\dagger}(\boldsymbol{r})|p^{-1}\rangle, \tag{13}$$

where $\phi_{\bar{K}}^{\dagger}$ is the meson creation operator, $|p^{-1}\rangle$ the proton-hole state, and E the kaon energy defined as $E = T_{\bar{K}} - T_p - S_p$ using the kinematical variables defined in the formation reaction, where $T_{\bar{K}}$ is the incident kaon kinetic energy, T_p the emitted proton kinetic energy, and S_p the proton separation energy from each proton single-particle level, which is compiled in Table III in Ref. [9] and in Table III in this article for various cases. The separation energies for the ground states of the daughter nuclei can be found in the *Table of Isotopes* [46]. Obtaining Green's function with the optical potential is essentially the same as solving the associated Klein-Gordon equation. We can calculate the nuclear response function $S(E)$ from $\tau_f^{\dagger}(\boldsymbol{r})G(E; \boldsymbol{r}, \boldsymbol{r}')\tau_f(\boldsymbol{r}')$ by performing the appropriate numerical integrations for the variables $\boldsymbol{r}$ and $\boldsymbol{r}'$.

In the Green's function formalism, we can calculate the response function $S(E)$ for both the bound and quasifree kaon production energy regions, and we can also perform the summation of the kaon final states without assuming the existence of discrete kaon bound states, which could disappear in the cases with a strongly absorptive optical potential.

As for the kaon-nucleus interaction, we mainly consider two different optical potentials: that obtained with the chiral unitary approach [28] and that obtained with a phenomenological fit [22]. We also consider another type of phenomenological potential in some cases for comparison, which was developed according to Ref. [38] to take into account the two-body kaon absorption effect explicitly. The optical potentials of the chiral unitary approach, which is obtained by the kaon self-energy in nuclear matter with the local density approximation, is described in detail in Ref. [28].

The optical potential obtained in the phenomenological fit [22] is written as

$$2\mu V_{\text{opt}} = -4\pi \eta a_{\text{eff}}(\rho)\rho(r), \tag{14}$$

where $a_{\text{eff}}(\rho)$ is a density-dependent effective scattering length and $\eta = 1 + m_{\bar{K}}/M_N$. The $a_{\text{eff}}(\rho)$ is parametrized as

$$\text{Re}\, a_{\text{eff}} = -0.15 + 1.66(\rho/\rho_0)^{0.24}\,\text{fm} \tag{15}$$

and

$$\text{Im}\, a_{\text{eff}} = 0.62 - 0.04(\rho/\rho_0)^{0.24}\,\text{fm}. \tag{16}$$

When we consider the atomic states, the energy dependence of the potentials considered in Ref. [13] is irrelevant because of the relatively small binding energies of the atomic states. We include the energy dependence of the phenomenological optical potentials in exactly the same manner as in Refs. [13, 47] whenever necessary.

Another type of phenomenological optical potential has the same real part as that of the phenomenological potential described above [Eq. (15)], but its imaginary part has a different form to show the two-body kaon absorption effect explicitly as explained in Ref. [38] in detail,

$$\text{Im}\, V_{\text{opt}} = -\frac{4\pi}{2\mu}\left\{\left(1 + \frac{m_{\bar{K}}}{m_N}\right)a_1\rho + \left(1 + \frac{m_{\bar{K}}}{2m_N}\right)a_2\rho^2\right\}. \tag{17}$$

Two parameter sets are newly determined to obtain a better χ^2 fit to the kaonic atom data for various nuclei than with the parameters listed in Ref. [38] where we only considered the $K^- - {}^{12}\text{C}$ system. One set is $(a_1, a_2) = (1.15, 66.8)$ in kaon mass units determined by assuming the kaon absorption from atomic $2p$ states [38], and another set is $(a_1, a_2) = (0.91, 136)$ in kaon mass units determined by assuming the kaon absorption from atomic $3d$ states [38]. In this article, we adopted the potential parameter $(a_1, a_2) = (1.15, 66.8)$. We use the same energy dependence of the potential as in Ref. [38] whenever necessary.

III. NUMERICAL RESULTS

First, we show plots of the calculated results of the density distributions of kaon bound states (Fig. 1) and of the (K^-, p) reaction spectra (Fig. 2) for kaonic atoms and kaonic nuclei formation of the $K^- - {}^{15}\text{N}$ system to explain the differences of the kaonic atoms and kaonic nuclei. Both states are solutions of the Klein-Gordon equation, Eq. (1), with the same optical potential. Thus, they should be called sequentially as $1s, 2s, 3s, \ldots$ for s-wave states, for example. However, since the real part of the optical potential is strongly attractive, there exist kaonic nuclear states bound in the interior of the nucleus which can be easily distinguished from the atomic "outer" states in the series of eigenstates of the same Hamiltonian, as we can see in Fig. 1, which shows the density distributions of the s-wave kaonic bound states in ${}^{15}\text{N}$. Both the ground state ($1s$) and the first excited state ($2s$) exist almost inside the nucleus, while the second excited state ($3s$) behaves like the ground state in the Coulomb potential and is usually recognized as the "ground state of kaonic *ATOMS*." As we can expect from the density distributions, the interior states ($1s$ and $2s$) and the outer state ($3s$) must have much different properties. Thus, we call the interior states "kaonic nuclei" and the outer states "kaonic atoms" to distinguish these states with significantly different character. This classification can be easily and unambiguously performed by observing the densities, for example, as shown in Fig. 1.
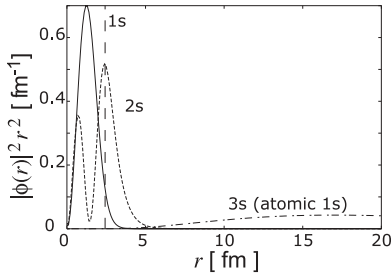
FIG. 1. Kaonic bound state density distributions $|\phi(r)|^2 r^2$ in coordinate space for ^{15}N obtained with the phenomenological optical potential [22]. The solid and dotted curves indicate the distributions of $1s$ and $2s$ states. The dashed curve represents the density of the $3s$ state which is usually regarded as a kaonic atom $1s$ state. The half-density radius of ^{15}N is also shown.

In Fig. 2, we show the calculated (K^-, p) reaction spectra for the formation of $K^- - {}^{15}$N bound systems. Here, we can also see the differences of the atomic states and nuclear states. In the spectra, the contributions of the formation of nuclear states distribute in a wide energy range such as $T_p = 600$–800 MeV and do not make any clear signals because of the large decay widths in our calculation. On the other hand, the atomic states have smaller binding energies and widths and make clear signals around the threshold $T_p \sim 590$ MeV shown as two spikes in Fig. 2. The detail structures of the spikes will be explained later. In this article, we mainly consider the structure and formation of these atomic outer states.

We solve the Klein-Gordon equation with the optical potential shown in Eq. (1) to obtain the binding energies and widths of the atomic states. The results for lighter nuclei were already compiled in Tables I and II of Ref. [9]. We show here the calculated results for heavier nuclei, ^{119}In and ^{207}Tl, which correspond to the kaon-nucleus systems formulated by the ^{120}Sn(K^-, p) and ^{208}Pb(K^-, p) reactions. We show the calculated binding energies and widths of kaonic atoms in Tables I and II for the phenomenological optical potential [22] and the chiral unitary optical potential [28], respectively. We also show the level structure of the kaonic atoms in ^{207}Tl in Fig. 3. As we found before in our previous paper [9], the

TABLE I. Calculated binding energies and widths of kaonic atoms in ^{119}In and ^{207}Tl with the phenomenological optical potential [22] in units of keV.

Atomic state (keV)	^{119}In		^{207}Tl	
	B.E.	Γ	B.E.	Γ
$1s$	4309.7	999.7	7279.9	1544.3
$2s$	2226.6	391.0	4194.2	711.5
$3s$	1376.8	194.7	2775.7	393.7
$4s$	938.2	111.0	1982.7	241.6
$2p$	3774.2	740.2	6779.2	1335.6
$3p$	2015.2	304.7	3962.3	629.2
$4p$	1270.5	156.4	2646.7	353.1
$3d$	2890.7	328.2	5853.3	896.4
$4d$	1658.7	160.2	3536.3	451.9
$4f$	1930.7	54.2	4629.0	434.4

TABLE II. Calculated binding energies and widths of kaonic atoms in ^{119}In and ^{207}Tl with the optical potential of the chiral unitary model [28] in units of keV.

Atomic state (keV)	^{119}In		^{207}Tl	
	B.E.	Γ	B.E.	Γ
$1s$	4296.8	944.5	7241.8	1502.7
$2s$	2226.2	366.7	4186.5	676.6
$3s$	1377.5	182.2	2774.5	372.0
$4s$	938.9	103.7	1983.1	227.8
$2p$	3778.4	681.0	6755.9	1270.8
$3p$	2020.5	279.9	3960.2	586.8
$4p$	1273.9	143.4	2648.5	328.1
$3d$	2888.2	303.8	5837.0	858.2
$4d$	1658.9	147.6	3532.9	424.0
$4f$	1930.9	48.4	4626.0	404.8

results obtained by both potentials resemble each other and, at the same time, indicate the existence of discrete deeply bound atomic states in all nuclei generally. For example, as shown in Fig. 3, the atomic $1s$, $2p$, $3d$ states overlap each other because of the level widths. However, we can also expect to have other narrow atomic states. Actually we should notice here that kaonic x-ray spectroscopy only provides data for the $7i$ state in this nuclear mass region. So, states deeper than the $7i$ state have not been observed so far and should be studied experimentally. As we mentioned above, the theoretical predictions are quite robust in this binding energy region and are quite reliable. Similar results for the atomic level structure with the phenomenological potential were also reported in Ref. [37].

To evaluate the formation spectra of these atomic states by the (K^-, N) reactions, we use the Green's function method. As we explained in Sec. II, in the (K^-, N) reactions, one nucleon is picked up and emitted from the target nucleus in the final states. We mainly consider here the (K^-, p) reaction. The deeper proton-hole states have large decay widths for γ decay and are not suited for the kaonic atom formation, because the widths of the proton-hole states can be significantly larger than the level spacing of kaonic atoms and can smear out all signals. Thus, we consider only the proton single-particle levels corresponding to the ground states of the daughter nuclei which do not have decay widths. We show in Table III the

TABLE III. One-proton separation energies S_p of ^{12}C, ^{16}O, ^{40}Ca, ^{120}Sn, and ^{208}Pb taken from Ref. [46]. All proton-holes in the final states correspond to the ground states of the daughter nuclei and have no decay widths.

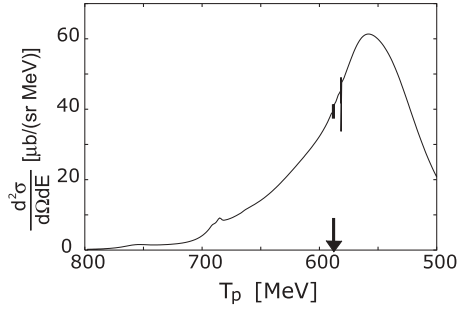|	Single-particle states	
Target	j_p	S_p [MeV]
^{12}C	$1p_{3/2}$	16.0
^{16}O	$1p_{1/2}$	12.1
^{40}Ca	$1d_{3/2}$	8.3
^{120}Sn	$1g_{9/2}$	10.7
^{208}Pb	$3s_{1/2}$	8.0

FIG. 2. Calculated spectra of the $^{16}O(K^-, p)^{15}N \otimes K^-$ reactions at $T_{\bar{K}} = 600$ MeV plotted as a function of the emitted proton energy T_p at $\theta_p^{lab} = 0°$. The energy-dependent phenomenological potential is used as in Ref. [13]. The arrow indicates the kaon production threshold.

FIG. 4. Momentum transfer in the $^{16}O(K^-, p)^{15}N \otimes K^-$ reactions. The proton separation energy S_p is fixed at 12.1 MeV, and the kaon binding energies are assumed to be 0, 50, and 100 MeV.

proton single-particle levels j_p and the separation energies S_p used in this paper, which are taken from Ref. [46].

As one can see in the studies of the deeply bound π atom formation reactions [10,12], the matching condition of the momentum transfer and the angular momentum transfer plays an important role in providing the large formation rate. As we can see from Table III, the target nuclei considered in this paper have various proton-hole states with different quantum numbers, and we can expect to have the interesting spectra with the characteristic behaviors for different targets. In Fig. 4, we show the momentum transfer of the $^{16}O(K^-, p)^{15}N \otimes K^-$ reactions as a function of the incident kaon kinetic energy for several kaon binding energy cases. We find that the recoilless condition is only satisfied for kaon bound states with relatively small binding energies (B.E. $\leqslant$ several MeV), for small incident kaon energies. For the states with large B.E., such as kaonic nuclear states, the recoilless condition is never satisfied; thus, the finite angular momentum transfer is preferred by the matching condition. For kaonic atoms, we can expect to have nearly recoilless kinematics for the small incident kaon energies. On the other hand, the momentum transfer is expected to be $q \sim 200$ MeV/c for the kaon energies obtained at the Japan Proton Accelerator Research Complex (J-PARC) facility.
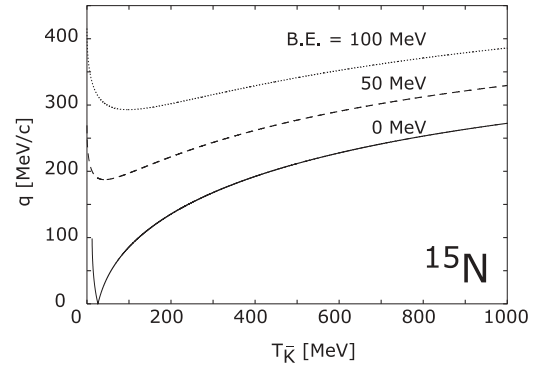
We show in Fig. 5 the calculated results of the kaonic atom formation spectra by an in-flight kaon beam for light nuclei. As reported in Ref. [13], we find very interesting shapes of the spectra for all nuclei. The calculated result for ^{12}C target with the chiral unitary optical potential (upper left figure in Fig. 5) is essentially the same as that in Fig. 5 in Ref. [13]. In this article, since we only include one proton-hole state in the final states corresponding to the ground states of the daughter nuclei, the absolute value of the cross sections are smaller than in the previous results [13].

As we can see from Fig. 5, the interesting structure of the spectra could be characterized by the angular momenta of the proton and kaon single-particle states. For the ^{12}C target case, the proton-hole state is considered to be $1p_{3/2}$. In this case, the subcomponents coupled with the $l_{\bar{K}} = 0$ states $(1s, 2s, \ldots)$ make the dips, while the subcomponents coupled with the $l_{\bar{K}} = 1$ states $(2p, 3p, \ldots)$ make the spectral shape with the steep rise and fall putting the resonance energy in between. We can see qualitatively the same characteristic shapes for the ^{16}O target case in Fig. 5, where the proton hole state is the $1p_{1/2}$ state. On the other hand, the spectral shape has different features for the ^{40}Ca target with the $1d_{3/2}$ proton-hole state in the daughter nucleus. In this case, the $l_{\bar{K}} = 1$ states show the
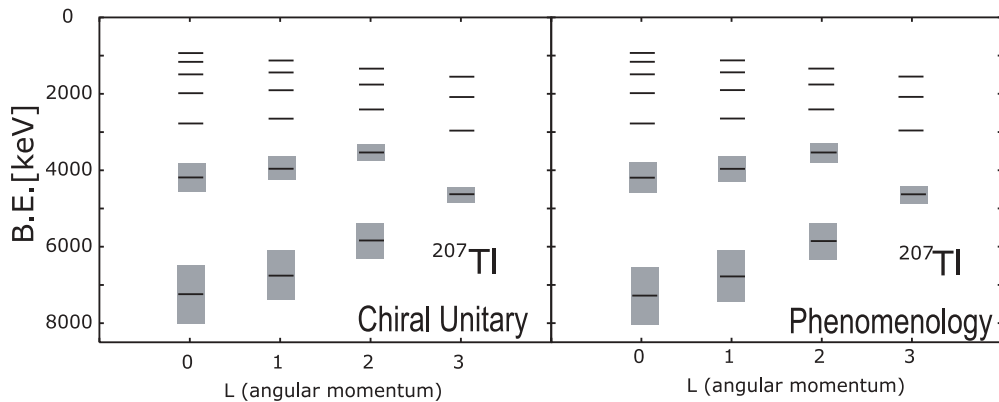

FIG. 3. Energy levels of kaonic atoms of ^{207}Tl up to the principle quantum number $n = 7$ obtained with the optical potentials of the chiral unitary model (left) and of the phenomenological fit (right). The hatched areas indicate the level widths for the deeply bound states such as B.E. >3 MeV.
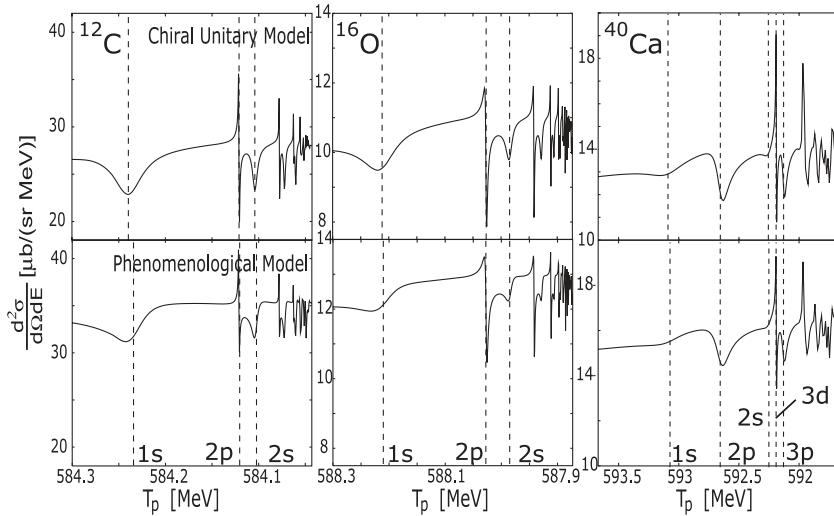
FIG. 5. Kaonic atom formation cross sections in (K^-, p) reactions at $T_{\bar{K}} = 600$ MeV for ^{12}C (left), ^{16}O (center), and ^{40}Ca (right) target nuclei plotted as functions of the emitted proton energy T_p at $\theta_p^{lab} = 0°$ for the chiral unitary potential (upper) [28] and for the phenomenological potential (lower) [22]. The vertical dashed lines indicate the binding energies of some kaonic atom states as indicated in the figure. The proton single-particle state considered for each target is ^{12}C $(1p_{3/2})$, ^{16}O $(1p_{1/2})$, and ^{40}Ca $(1d_{3/2})$, as listed in Table III.

dip structure and the $l_{\bar{K}} = 2$ state has the spectral shape with the steep rise and fall. As for the origin of these interesting spectral shapes, we will offer some discussion in Sec. IV B.

In Fig. 5, we can also see that the formation spectra calculated with the phenomenological optical potential and the chiral unitary potential are qualitatively the same. Thus, we can expect that the theoretical predictions are quite robust for these potentials. On the other hand, to distinguish the different potentials, we need very precise data which enable us to recognize the tiny differences appearing between the upper and lower figures in Fig. 5.

In Fig. 6, we also consider the heavier target cases, ^{120}Sn and ^{208}Pb. The reason to consider the heavier targets is to

FIG. 6. Kaonic atom formation cross sections in (K^-, p) reactions at $T_{\bar{K}} = 600$ MeV for ^{120}Sn and ^{208}Pb target nuclei plotted as functions of the emitted proton energy T_p at $\theta_p^{lab} = 0°$ for the chiral unitary potential (upper) [28] and the phenomenological potential (lower) [22]. The vertical dashed lines indicate the binding energies of some kaonic atom states for ^{120}Sn as indicated in the figure. For ^{208}Pb, the bound states up to $4d$ do not show clear indications in the spectra. The proton single-particle state considered for each target is ^{120}Sn $(1g_{9/2})$ and ^{208}Pb $(3s_{1/2})$ as listed in Table III.

investigate the spectral shapes with different proton single-particle levels, $1g_{9/2}$ for ^{120}Sn and $3s_{1/2}$ for ^{208}Pb, and to study the possibility of observing very deeply bound kaonic atoms. Actually, for the heavier nuclei, the atomic level spacing is expected to be larger in general than in lighter nuclei because of the Coulomb-like level structure, and thus the very high energy resolution could be unnecessary to observe the peaks in the formation spectra and to distinguish the results with both potentials.

As we can see in Fig. 6, the level spacing and width of each peak structure are larger for heavier targets cases than for lighter targets shown in Fig. 5 as we expected. The spectrum for the ^{120}Sn target case, where the proton $1g_{9/2}$ state is considered, shows the qualitatively same structure as that for the ^{40}Ca target with the $1d_{3/2}$ proton state and has the dips of the $l_{\bar{K}} = 1$ states and the shape with the rise and fall of $l_{\bar{K}} = 2$. For the ^{208}Pb target case, we can only observe the clear signals for the formation of shallow atomic states at $T_{\bar{K}} = 600$ MeV. The bound states up to $4d$ do not show the clear indications due to the large widths and the large momentum transfer. In both target cases, the shapes of the calculated spectra of both potentials, chiral unitary model and phenomenological model, resemble each other, and it seems difficult to distinguish these potentials by the observed spectra.

Finally, we show the calculated results for the lower kaonic incident energy cases to know the spectra with the recoilless condition. In Fig. 7, we show the calculated spectra for the ^{208}Pb target. Here, as shown in Eqs. (7) and (8), we have not included Coulomb distortion for the emitted proton in our calculation, which could reduce the absolute cross sections for the lower proton energy cases. In the recoilless kinematics, the kaonic states with small angular momenta are expected to be largely populated with the $s_{1/2}^{-1}$ proton hole for the ^{208}Pb target because of the matching condition. Actually, the s and d kaonic state contributions dominate the spectra. The kaonic p states are suppressed by parity. We have found that the calculated spectra with the recoilless condition shown in Fig. 7 are significantly different from those with the in-flight kaon cases shown in Fig. 6 (right) and have found that the deeper kaonic states with lower angular momenta provide clear structures in the spectra. Hence, we think that the atomic states
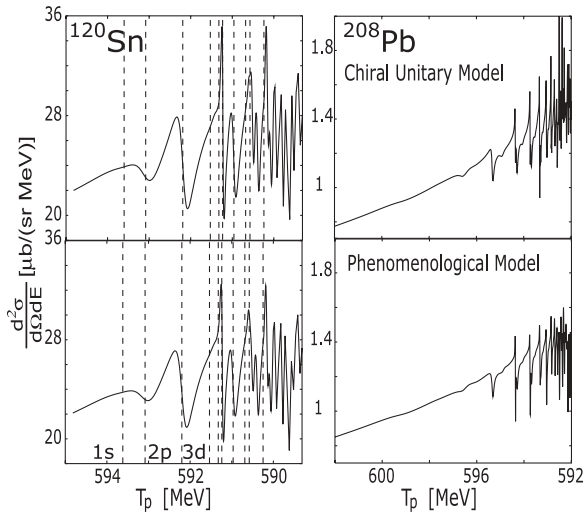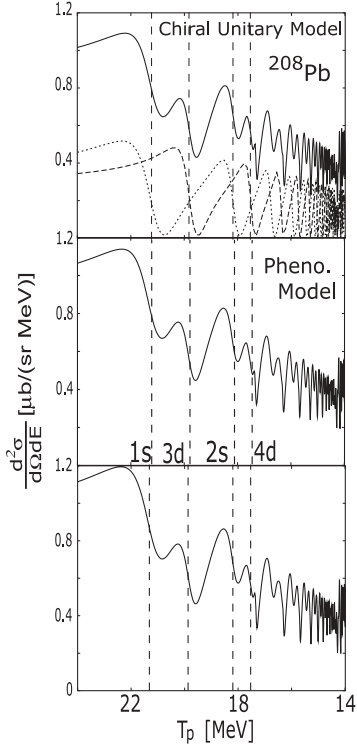
FIG. 7. Kaonic atom formation cross sections in ^{208}Pb(K^-, p) reactions at $T_{\bar{K}} = 22$ MeV, which correspond to the recoilless kinematics for the ^{208}Pb target, plotted as function of the emitted proton energy T_p at $\theta_p^{\mathrm{lab}} = 0°$ for the chiral unitary potential (upper) [28], for the phenomenological potential (middle) [22], and another phenomenological potential defined in Eq. (17) with the parameters, $(a_1, a_2) = (1.15, 66.8)$ in kaon mass units (lower). The dotted and dashed curves in the upper figure indicate the subcomponents of s- and d-wave kaonic atom states, respectively, and the vertical dashed lines indicate the binding energies of s- and d-wave kaonic atom states. The proton single-particle state considered is $3s_{1/2}$ as listed in Table III.

formation with the recoilless kinematics using the low energy kaon is also interesting in the study of deeply bound kaonic atoms. On the other hand, as shown in Fig. 7, we have found again that the differences of the expected spectra due to those of the kaon-nucleus optical potential are tiny at the recoilless kinematics case.

IV. DISCUSSIONS

A. Effects of the existence of kaonic nuclei

In this section, we would like to explore the possible effects to the (K^-, p) spectra in the energy region of the atomic states formation due to the existence of kaonic nuclear states. As we discussed in the beginning of Sec. III, the kaonic nuclear states and kaonic atom states are the eigenstates of the same Hamiltonian, and their wave functions are expected to satisfy the orthogonality condition.[1] Thus, if there exist kaonic nuclear states, the wave functions of the kaonic atom states have nodes

inside the nucleus to satisfy the orthogonality conditions with kaonic nuclear states.

On the other hand, the spatial dimensions of the kaonic nuclear states are almost equivalent to those of nucleons in the nucleus. Hence, we can expect that the wave functions of nucleons and kaonic nuclear states with the same quantum numbers resemble each other, which means that the nucleon wave functions may satisfy the orthogonality conditions approximately with outer kaonic atom wave functions.

For example, we consider the K^--^{39}K system with the phenomenological optical potential, which has several kaonic nuclear states $1s, 2s, 2p, \ldots$ as listed in Table I in Ref. [9]. Thus, the kaonic atom wave functions of the system are expected to be approximately orthogonal to kaonic nuclear wave functions and also to the nuclear wave functions with the same principal quantum number n and orbital angular momentum l.

Another important thing is that the strength of the formation of kaonic atoms can be simply estimated by the effective number approach adopted in Refs. [9,10], which can be roughly described as

$$N_{\mathrm{eff}} \propto \left| \int d\boldsymbol{r} \exp(i\boldsymbol{q} \cdot \boldsymbol{r}) D(\boldsymbol{b}) \phi_{\bar{K}}^* \psi_N \right|^2, \quad (18)$$

with the momentum transfer $\boldsymbol{q}$, the distortion factor $D(\boldsymbol{b})$, and the wave functions of kaon and nucleon $\phi_{\bar{K}}^*$ and ψ_N [9,10]. This factor can be reduced to the simpler form

$$N_{\mathrm{eff}} \propto \left| \int d\boldsymbol{r} \, \phi_{\bar{K}}^* \psi_N \right|^2, \quad (19)$$

by considering the recoilless kinematics ($\mathbf{q} \sim 0$) and neglecting the distortion effect, which will be 0 for the orthogonal sets of the wave functions. Thus, we can conclude that the existence of the kaonic nuclear states may significantly reduce the formation rate of kaonic atom states coupled to the nucleon hole states with the same quantum (nl) numbers of the kaonic nuclei in the recoilless kinematics.

We show the numerical results of these scenarios for some cases below. We consider the (K^-, n) reactions for ^{40}Ca and ^{16}O targets. The valence neutron states are $2s_{1/2}$ for ^{40}Ca and $1p_{1/2}$ for ^{16}O, respectively. As shown in Tables I and II in Ref. [9], we expect to have a kaonic nuclear $2s$ state for $A \sim 40$ nuclei with the phenomenological deep optical potential, while we do not expect the $2s$ kaonic states with the chiral unitary optical potential. Similarly, we expect a kaonic nuclei p state for $A \sim 16$ nuclei with the phenomenological potential but not with the chiral unitary potential. Thus, as described above, we can expect a significant suppression of the atomic state formation cross sections for the calculations with the phenomenological optical potential because of the approximate orthogonality between kaonic atom wave functions and valence neutron wave functions at the recoilless kinematics.

The numerical results are shown in Fig. 8. In the upper panels, we calculate the spectra by neglecting the distortion

---

[1]Strictly speaking, this orthogonal condition holds only approximately for the Klein-Gordon equation, Eq. (1), and should be modified

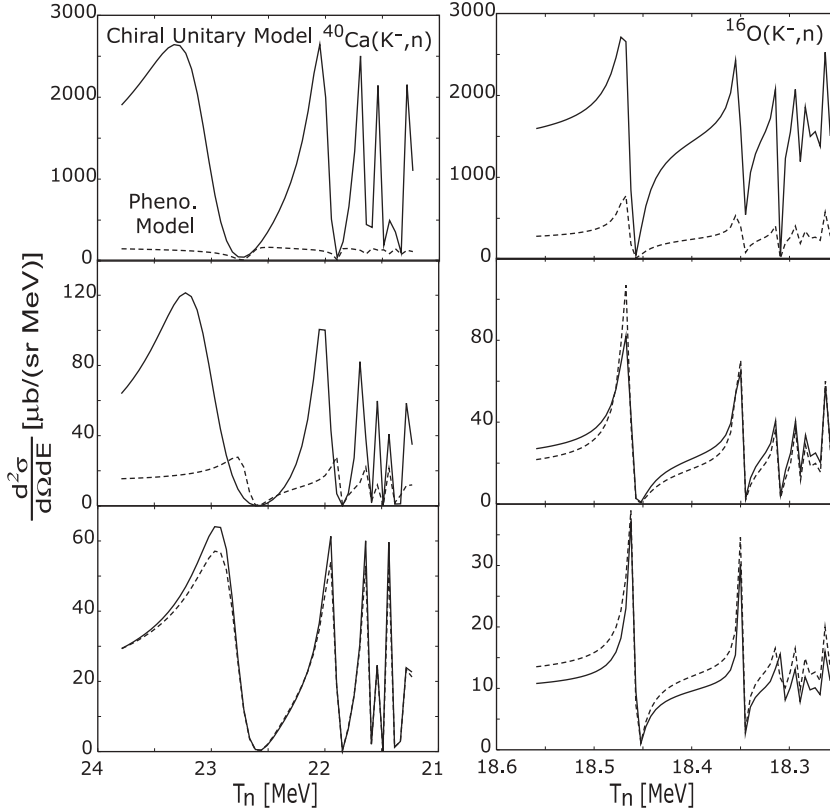from its usual form because of the existence of the energy dependence and the imaginary part of the optical potential [48].

FIG. 8. Kaonic atom formation cross sections in ^{40}Ca(K^-, n) and ^{16}O(K^-, n) reactions at recoilless kinematics using low energy kaon beams with $T_{\bar{K}} = 39.4$ MeV for the ^{40}Ca target and $T_{\bar{K}} = 33.9$ MeV for the ^{16}O target. The cross sections are plotted as the functions of the emitted neutron energy T_n at $\theta_n^{\text{Lab}} = 0°$ for the chiral unitary potential (solid line) [28] and the phenomenological potential (dashed line) [22]. The spectra are calculated with (upper panels) no distortion effects [$F(\mathbf{r}) = 1$ in Eq. (7)] and the reduced imaginary potentials Im $V/5$, (middle panels) full distortion effects and the reduced imaginary potentials Im $V/5$, and (lower panels) full distortion effects and full imaginary potentials corresponding to the full calculation in our model. The neutron separation energies S_n are 18.1 MeV for ^{40}Ca and 15.7 MeV for ^{16}O.

effects and by reducing the strength of the imaginary part of the optical potentials to Im $V_{\text{opt}}/5$ to confirm our expectation in the ideal cases. We found that our expectation is correct, and the spectra with the phenomenological optical potential is suppressed significantly in both target cases. The spectra with the chiral unitary potential, which do not provide the kaonic nuclear states with the same quantum number as the valence neutron states, have significantly larger absolute values than those with the phenomenological potential, as expected. Now, we move to the realistic calculations. In the middle panels, we show the spectra with the full distortion effects and the reduced imaginary optical potentials Im$V_{\text{opt}}/5$. We found that the significant differences of the spectra due to the optical potential remain for the ^{40}Ca target case, while the differences disappeared for the ^{16}O target case because of the distortion effects.

In the lower panels, we show the results with the full calculation of our model with the full distortion effects and the full imaginary part of the optical potentials. We found that the discrepancies of the spectra for the ^{40}Ca target also disappeared by including the full imaginary part of the optical potentials, and the spectra with the different optical potentials resemble each other for both target cases.

Hence, we think that our idea is nice and reasonable; however, it does not work well for kaon-nucleus systems because of the strong absorption effects and the distortion effects of the reaction. Thus, our idea could be realized in cases with less absorptive system formation by reactions with particles with smaller distortion effects.

B. Origin of the interesting spectra shape of atomic state formation

In this section, we consider the origin of the interesting structures of the formation spectra of the kaonic atom states. We follow the discussions given in Ref. [6] and show a simple example.

In the Green's function formalism, we can divide Green's function into two parts, the pole part G_{pole} and the background part G_{BG}, as

$$G(E) = G_{\text{pole}}(E) + G_{\text{BG}}(E), \qquad (20)$$

where the pole part can be written as

$$G_{\text{pole}} = \frac{1}{E - (\epsilon - i\Gamma/2)}[\text{res } G(E)|_{E=\epsilon-i\Gamma/2}], \qquad (21)$$

where $\epsilon - i\Gamma/2$ is the complex pole energy. The contribution to the spectra from the pole part can be expressed as

$$S_{\text{pole}}(E) = -\frac{1}{\pi}\text{Im}\frac{A}{E - (\epsilon - i\Gamma/2)}, \qquad (22)$$

where A is defined as

$$A = \sum_f \tau_f^+[\text{res } G(E)|_{E=\epsilon-i\Gamma/2}]\tau_f, \qquad (23)$$

with τ_f defined in Eq. (6). The magnitude A includes the information of the residue of Green's function and the wave functions of the particles participating in the formation reactions. As a simple example, we write the argument of A as
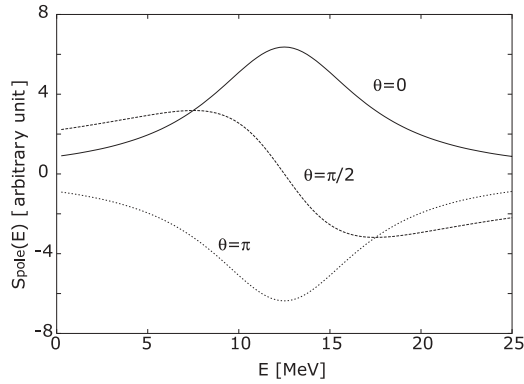
FIG. 9. Contribution to the spectra from the pole S_{pole} as function of E. The pole energy is assumed to be $E = 12.5 - 5i$ MeV. These lines indicate the S_{pole} behavior with the arg $A = 0, \pi/2$, and π, where A is defined in Eq. (23).

$\theta = \arg A$ and plot in Fig. 9 the S_{pole} contribution in Eq. (22) for three θ values.

We have found that the shape of the formation spectra of the bound states changes according to the argument θ of A, and we have the resonance peak structure for $\theta = 0$, the spike structure with the rise and fall of the spectrum for $\theta = \pi/2$, and the resonance dip for $\theta = \pi$.

Thus, we can deduce the information of the phase of A in Eq. (23) from the shape of the spectra. On the other hand, the simple fit by a Lorentz distribution is not suited for these spectra, and we should be careful to extract the resonance energies and the widths from the data. This interference of the pole contribution with the background also appeared in the case of pionic atoms production in the $\gamma A \to \gamma A_\pi$ reaction in Ref. [49].

V. CONCLUSION

We study the formation spectra of the deeply bound kaonic atoms theoretically in this paper. The deeply bound atomic states cannot be observed by the standard x-ray spectroscopy; however, theoretical calculations have shown the existence of the narrow (quasistable) bound states beyond the accessible levels by the x-ray method. We show the calculated results of the binding energies and widths of the deeply bound kaonic atom states with the phenomenological and the chiral unitary optical potentials.

We consider the missing mass spectroscopy by the (K^-, N) reactions as the formation reactions of the deeply bound states. We study various target nuclei and different incident energies and systematically show the expected (K^-, p) spectra; we also consider (K^-, n) reactions in several cases. We then compare the expected spectra of the different optical potentials obtained by the phenomenological fit and the chiral unitary model. We have found that the expected spectra always show interesting structures for various target cases with clear signals of the atomic state formation.

The origin of the interesting structure is also considered. We show that the argument of the pole contribution of the spectral function is important and we should be careful to deduce the resonance energies and widths from the data.

The effects due to the existence of the kaonic nuclear states are also investigated. We show that the exotic nuclear states with less absorptive interaction will be identified by observing the atomic states by the missing mass spectroscopy using the transport particles at the recoilless kinematics.

Finally, we would like to comment on the importance of the experimental investigations of this research. As shown in this article, the structures of the deeply bound kaonic atoms are very robust, and all optical potentials, which reproduce the existing weakly bound atomic data, are expected to provide similar predictions for the deeply bound atomic states. Thus, experimentally confirming the predicted structures is of great importance, since all present potentials reproducing the lightly bound kaonic atoms make the same prediction for the spectra of the (K^-, p) reaction in the deeply bound K^- atom region. If an experiment with enough resolution did not find the predicted structures, this would cast serious doubt on the validity of such potentials. This could happen if we have all missed the important ingredients of the kaon-nucleus interactions for higher densities. Thus, we think that it is very important to experimentally investigate the structures of the deeply bound kaonic atoms. We hope that our results stimulate the experimental study of the deeply bound kaonic atoms, even though it is very hard to observe these states.

[1] Y. Akaishi and T. Yamazaki, Phys. Rev. C **65**, 044005 (2002); A. Doté, H. Horiuchi, Y. Akaishi, and T. Yamazaki, Phys. Lett. **B590**, 51 (2004).

[2] M. Agnello *et al.*, Phys. Rev. Lett. **94**, 212303 (2005); M. Agnello *et al.*, Nucl. Phys. **A775**, 35 (2006).

[3] E. Oset and H. Toki, Phys. Rev. C **74**, 015207 (2006); V. K. Magas, E. Oset, A. Ramos, and H. Toki, *ibid*. **74**, 025206 (2006).

[4] M. Iwasaki *et al.*, arXiv:nucl-ex/0310018; T. Suzuki *et al.*, Phys. Lett. **B597**, 263 (2004); Nucl. Phys. **A754**, 375c (2005).

[5] M. Iwasaki, talks at Japan Physical Society Meeting, Nara, Japan, Sept. 2006 and at YKIS 2006, Kyoto, Japan, Dec. 2006 (unpublished); H. Outa, talk at Korean Physical Society Meeting, Daegu, Korea, Oct. 2006 (unpublished).

[6] O. Morimatsu and K. Yazaki, Nucl. Phys. **A435**, 727 (1985); **A483**, 493 (1988).

 [7] T. Kishimoto, Phys. Rev. Lett. **83**, 4701 (1999).

 [8] E. Friedman and A. Gal, Nucl. Phys. **A658**, 345 (1999).

 [9] J. Yamagata, H. Nagahiro, Y. Okumura, and S. Hirenzaki, Prog. Theor. Phys. **114**, 301 (2005); **114**, 905(E) (2005).

[10] S. Hirenzaki, H. Toki, and T. Yamazaki, Phys. Rev. C **44**, 2472 (1991); H. Toki, S. Hirenzaki, and T. Yamazaki, Nucl. Phys. **A530**, 679 (1991).

[11] H. Toki and T. Yamazaki, Phys. Lett. **B213**, 129 (1988); H. Toki, S. Hirenzaki, R. S. Hayano, and T. Yamazaki, Nucl. Phys. **A501**, 653 (1989).

[12] H. Gilg *et al.*, Phys. Rev. C **62**, 025201 (2000); K. Itahashi *et al.*, *ibid.* **62**, 025202 (2000).

[13] J. Yamagata, H. Nagahiro, and S. Hirenzaki, Phys. Rev. C **74**, 014604 (2006).

[14] K. Ikuta, M. Arima, and K. Masutani, Prog. Theor. Phys. **108**, 917 (2002); T. Koike and T. Harada, Phys. Lett. **B652**, 262 (2007).

[15] T. Kishimoto *et al.*, Prog. Theor. Phys. Suppl. **149**, 264 (2003); T. Kishimoto *et al.*, Nucl. Phys. **A754**, 383c (2005).

[16] T. Kishimoto *et al.*, Prog. Theor. Phys. **118**, 181 (2007); talks at KPS, Daegu, Korea, Oct. 2006, at YKIS, Kyoto, Japan, Dec. 2006, and at INPC07, Tokyo, Japan, June 2007 (unpublished).

[17] D. Jido, J. A. Oller, E. Oset, A. Ramos, and U. G. Meissner, Nucl. Phys. **A725**, 181 (2003).

[18] V. K. Magas, E. Oset, and A. Ramos, Phys. Rev. Lett. **95**, 052301 (2005).

[19] M. Alberg, E. M. Henley, and L. Wilets, Ann. Phys. (NY) **96**, 43 (1976).

[20] R. Brockmann, W. Weise, and L. Tauscher, Nucl. Phys. **A308**, 365 (1978).

[21] M. Mizoguchi, S. Hirenzaki, and H. Toki, Nucl. Phys. **A567**, 893 (1994).

[22] C. J. Batty, E. Friedman, and A. Gal, Phys. Rep. **287**, 385 (1997).

[23] R. H. Dalitz, T. C. Wong, and G. Rajasekaran, Phys. Rev. **153**, 1617 (1967).

[24] N. Kaiser, P. B. Siegel, and W. Weise, Nucl. Phys. **A594**, 325 (1995).

[25] E. Oset and A. Ramos, Nucl. Phys. **A635**, 99 (1998).

[26] T. Waas, N. Kaiser, and W. Weise, Phys. Lett. **B365**, 12 (1996); **B379**, 34 (1996); T. Waas and W. Weise, Nucl. Phys. **A625**, 287 (1997).

[27] M. Lutz, Phys. Lett. **B426**, 12 (1998).

[28] A. Ramos and E. Oset, Nucl. Phys. **A671**, 481 (2000).

[29] A. Cieplý, E. Friedman, A. Gal, and J. Mareš, Nucl. Phys. **A696**, 173 (2001).

[30] L. Tolos, A. Ramos, and E. Oset, Phys. Rev. C **74**, 015203 (2006).

[31] C. Garcia-Recio, E. Oset, A. Ramos, and J. Nieves, Nucl. Phys. **A703**, 271 (2002).

[32] L. Tolós, A. Ramos, A. Polls, and T. T. S. Kuo, Nucl. Phys. **A690**, 547 (2001).

[33] L. Tolós, A. Ramos, and A. Polls, Phys. Rev. C **65**, 054907 (2002).

[34] J. Schaffner-Bielich, V. Koch, and M. Effenberger, Nucl. Phys. **A669**, 153 (2000).

[35] S. Hirenzaki, Y. Okumura, H. Toki, E. Oset, and A. Ramos, Phys. Rev. C **61**, 055205 (2000).

[36] A. Baca, C. García-Recio, and J. Nieves, Nucl. Phys. **A673**, 335 (2000).

[37] E. Friedman and A. Gal, Phys. Lett. **B459**, 43 (1999).

[38] J. Yamagata and S. Hirenzaki, Eur. Phys. J. A **31**, 255 (2007).

[39] J. Nieves, E. Oset, and C. Garcia-Recio, Nucl. Phys. **A554**, 509 (1993).

[40] E. Oset and L. L. Salcedo, J. Comput. Phys. **57**, 361 (1985).

[41] R. S. Hayano, S. Hirenzaki, and A. Gillitzer, Eur. Phys. J. A **6**, 99 (1999).

[42] F. Klingl, T. Waas, and W. Weise, Nucl. Phys. **A650**, 299 (1999); E. Marco and W. Weise, Phys. Lett. **B502**, 59 (2001).

[43] D. Jido, H. Nagahiro, and S. Hirenzaki, Phys. Rev. C **66**, 045202 (2002); H. Nagahiro, D. Jido, and S. Hirenzaki, *ibid.* **68**, 035205 (2003); Nucl. Phys. **A761**, 92 (2005).

[44] H. Nagahiro and S. Hirenzaki, Phys. Rev. Lett. **94**, 232503 (2005); H. Nagahiro, M. Takizawa, and S. Hirenzaki, Phys. Rev. C **74**, 045203 (2006).

[45] B. Conforto *et al.*, Nucl. Phys. **B105**, 189 (1976).

[46] *Table of Isotopes*, 8th ed., edited by R. B. Firestone *et al.* (Wiley, New York, 1996).

[47] J. Mareš, E. Friedman, and A. Gal, Phys. Lett. **B606**, 295 (2005); Nucl. Phys. **A770**, 84 (2006).

[48] N. Nose-Togawa, S. Hirenzaki, and K. Kume, Nucl. Phys. **A623**, 548 (1997).

[49] R. C. Carrasco, J. Nieves, and E. Oset, Nucl. Phys. **A565**, 797 (1993).